

# Iterative Decoder of Channel-polarized Multilevel Coding for Data Center Networks

Takeshi Kakizaki, Masanori Nakamura, *Member, IEEE*, Fukutaro Hamaoka, *Member, IEEE*,  
Shuto Yamamoto, *Member, IEEE*, and Etsushi Yamazaki, *Member, IEEE*

**Abstract**—Data center networks (DCNs) require a low-cost, low-power optical transceiver to handle increased traffic from generative artificial intelligence, video streaming services, and more. Improving the required signal-to-noise ratio (RSNR) by digital signal processing such as forward error correction (FEC) mitigates the requirements for electrical and optical components. The optical transceivers in DCNs exploit a low-complexity soft-decision (SD) FEC, consisting of short block-length linear error-correcting codes and a low-complexity SD decoder (SDD), such as a Chase decoder and ordered statistical decoding. The low complexity SDD efficiently approaches a maximum likelihood decoding (MLD). However, the decoding performance of MLD is limited by its finite block length. In this paper, we describe the detail of our proposed channel-polarized multilevel coding with iterative decoding (CP-MLC-ID), which improves the decoding performance. The 19.5%-OH CP-MLC-ID 128-bit extended Bose-Chaudhuri-Hocquenghem (eBCH) and KP4 codes outperform the concatenated eBCH and KP4 codes with a net coding gain of 0.25 and 0.40 dB for the same and double the number of SDDs, respectively. We also investigate the dependency of the decoding performance on the size of a bit interleaver. The performance degradation of CP-MLC-ID using an 8-bit interleaver is about 0.1 dB compared to using the large-bit interleaver. Our results indicate that even a weak connection by exclusive-OR between codewords improves the decoding performance, compared to simple concatenated codes in the DCNs.

**Index Terms**—optical communication, forward error correction, multilevel coding.

## I. INTRODUCTION

INTERNET traffic has been increasing rapidly to keep up with generative artificial intelligence, video streaming services, and more. Digital coherent optical communication systems have recently been deployed in intra- and inter-data center networks (DCNs) in addition to metro and core networks to achieve cost- and energy-efficient networks [1], [2]. The optical transceivers in DCNs exploit a low-complexity soft-decision forward error correction (SD-FEC) scheme that consists of a pair of short block length codes and low-complexity SD decoding (SDD) to maintain reliable communication with the low power consumption of the optical transceiver. Vendors are developing the *cFEC*, which consists of the concatenated Hamming and staircase codes, for <120-km optical links for 400 Gbps [3]. Novel O-band <10-km optical links for 800 Gbps adopt the concatenated codes, consisting of an inner Bose–Chaudhuri–Hocquenghem (BCH) and

outer KP4 codes, called LR-FEC. Vendors are also considering adopting the LR-FEC for the <120-km optical link for a 1.6-Tbps application in the *Optical Internetworking Forum* [4]–[7].

A low-complexity SD-FEC provides middle decoding performance with low power consumption because the low-complexity SDD efficiently approaches the maximum likelihood decoding (MLD) by searching the codewords around the received signals. However, the decoding performance is limited by the block length due to increasing the decoding complexity of low-complexity SDD in proportion to the minimum distance between codewords or the overhead (OH) [8]–[10]. To improve the performance-complexity tradeoff, the iterative decoding of short block length inner and outer codes has been developed. The LR-FEC with iterative decoding provides the pre-FEC BER threshold of  $1.6 \times 10^{-2}$  compared to the conventional one of  $1.2 \times 10^{-2}$  to achieve a post-BER of  $10^{-15}$ ; however, this comes at the cost of doubling the number of iterations [7].

As an alternative, the channel-polarized multilevel coding (CP-MLC) with low-complexity SDD and low-OH inner codes can improve the decoding complexity at the middle BER region such as the KP4 BER threshold [11], [12]. The CP-MLC converts a  $d$  discrete memoryless channel ( $W_1, W_2, \dots, W_d$ ) into  $(V_1, V_2, \dots, V_d)$ , where we denote the unreliable bit channel  $V_1$  and the reliable bit channels  $V_j$  for each  $2 \leq j \leq d$ , and only applies the SDD in the unreliable bit channels  $V_1$  [13], [14]. However, the CP-MLC with a high OH region cannot efficiently achieve the target BER in the middle BER region due to the error floor caused by bypassing SDD on the reliable bit channels  $V_j$ .

To improve the decoding performance in the high OH and middle BER region, we proposed CP-MLC with iterative decoding (CP-MLC-ID), which uses the channel conversion ( $W_1, W_2, \dots, W_d$ ) into  $(U_1, U_2, \dots, U_d)$ , where we denote a  $d - 1$  unreliable bit channel  $U_j$  for each  $1 \leq j \leq d - 1$  and highly reliable bit channel  $U_d$  instead of the channel conversion of CP-MLC, and uses iterative decoding [15], [16]. The CP-MLC-ID with BCH and KP4 codes can improve the performance-complexity tradeoffs compared to concatenated BCH-KP4 codes and reduce the error floor in the highly reliable bit channel  $U_d$ .

In this paper, we explain the details of CP-MLC-ID as an expansion of [15], [16], including a discussion of the interleaver design and dependency. We show that a roughly 19.5% CP-MLC-ID can exceed the NCG with the same complexity and the maximum NCG by 0.25 and 0.4 dB, respectively, compared to concatenated codes. In practice, we

T. Kakizaki, M. Nakamura, F. Hamaoka, S. Yamamoto, Etsushi Yamazaki are NTT Network Innovation Laboratories, Nippon Telegraph and Telephone Corporation, Yokosuka-shi, Kanagawa 239-0847, Japan, e-mail: takeshi.kakizaki@ntt.com

Manuscript received April 19, 20XX; revised August 26, 20XX.

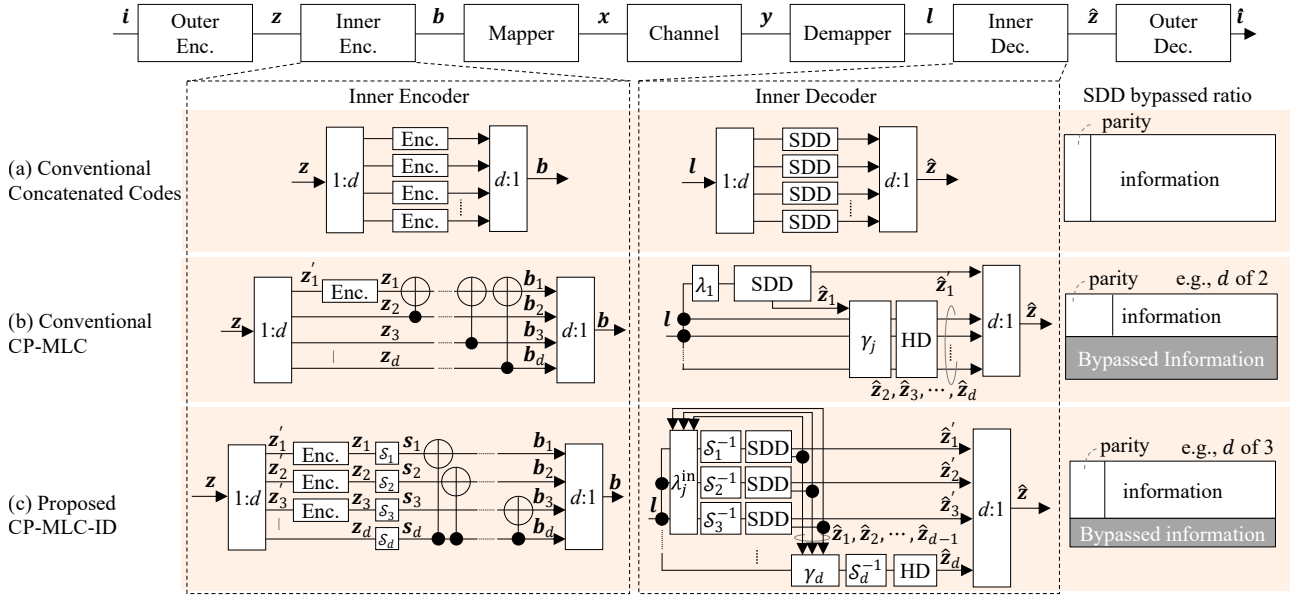


Fig. 1. Schematic diagrams of (a) conventional concatenated codes, (b) conventional CP-MLC, and (c) proposed CP-MLC-ID.

also investigate the performance degradation for CP-MLC-ID with 128-bit extended BCH (eBCH) codes, which is about 0.1 dB for a bit interleaver size of 8 bits. CP-MLC-ID, which exploits a weak connection by exclusive-OR between codewords, can improve the decoding performance compared to simple concatenated codes.

Sec. II of this paper explains the conventional concatenated codes and CP-MLC. In Sec. III, we describe the encoder, decoder, and interleaver design of CP-MLC-ID. In Sec. IV, we evaluate the decoding performance and the decoding complexity of concatenated codes, CP-MLC, and CP-MLC-ID. We conclude in Sec. V with a brief summary.

## II. SYSTEM MODEL AND CONVENTIONAL CODES FOR DCNS

### A. Concatenated codes

This section describes the concatenated codes for the DCNs. Figure 1 (a) shows a schematic diagram of the inner encoder and decoder for the concatenated codes. First, the encoder converts the information bits  $u \in \{0, 1\}^k$  into the outer codeword  $z \in \{0, 1\}^{n_{\text{HD}}}$ , and the inner encoder converts the outer codeword  $z$  into inner codewords  $b \in \{0, 1\}^n$ . We assume that the modulation format is a *binary phase shift keying* (BPSK), i.e., the symbol mapper transforms  $b$  into the symbols  $x = 1 - 2b$ . A received signal is given by  $y \triangleq x + e$ , where  $e \in \mathbb{R}^n$  is a vector of additive white Gaussian noise (AWGN). The output of the demapper is the log-likelihood ratio (LLR) of  $l \triangleq 2y/\sigma^2$ .

The concatenated codes can efficiently correct the large bit error by the inner SDD and the residual error by the outer hard-decision decoder (HDD). The performance of low-complexity SDD (e.g., Chase2 decoder and OSD) can approach that of the MLD, which can achieve the optimal block error rate for SDD, while the MLD is not optimal for the bit error rate (BER) [17].

### B. Channel-polarized multilevel coding

In this section, we explain the encoder and decoder of CP-MLC [13], [14]. The CP-MLC can improve the decoding performance of BER compared to the concatenated codes with near MLD under some BER regions [12].

Figure 1 (b) shows a schematic diagram of the CP-MLC encoder and decoder. The encoder first calculates the outer codeword  $z \triangleq (z_1, z_2, \dots, z_d)$ , where  $z_1 \in \{0, 1\}^{nR_1/d}$ ,  $z_2, \dots, z_d \in \{0, 1\}^{n/d}$ . The inner encoder transforms  $z_1'$  into  $z_1 \in \{0, 1\}^{n/d}$ , where  $n$  and  $R_1$  indicate the block length and the coding rate of the inner and outer code, respectively. The encoder then converts  $(z_1, z_2, \dots, z_d)$  into

$$(b_1, b_2, \dots, b_d) \triangleq (z_1 \oplus z_2 \oplus \dots \oplus z_d, z_2, \dots, z_d), \quad (1)$$

where  $a \oplus b$  is the XOR for each element of a vector.

On the decoder side, the decoder first calculates the estimated codeword  $\hat{z}_1$  and information bits  $\hat{z}_1'$  from the unreliable LLR (uLLR), as

$$\lambda_1(l) \triangleq \log \frac{P_{Z_1}(0)}{P_{Z_1}(1)} + \log \frac{P_{\underline{L}|Z_1}(l|0)}{P_{\underline{L}|Z_1}(l|1)} \quad (2)$$

$$= l_1 \boxplus l_2 \boxplus \dots \boxplus l_d, \quad (3)$$

where we define

$$\underline{l} \triangleq (l_1, l_2, \dots, l_d) \quad (4)$$

and

$$a \boxplus b \triangleq 2 \tanh^{-1} \left( \tanh \frac{a}{2} \cdot \tanh \frac{b}{2} \right). \quad (5)$$

Next, the estimated bits  $z_2, z_3, \dots, z_d$  are calculated from  $\hat{z}_j = 0.5(1 - \gamma_j(\underline{l}, \hat{z}_1))$  by using the reliable LLR (rLLR), as

$$\gamma_j(\underline{l}, z_1) \triangleq \log \frac{P_{Z_j}(0)}{P_{Z_j}(1)} + \log \frac{P_{\underline{L}, Z_1|Z_j}(\underline{l}, z_1|0)}{P_{\underline{L}, Z_1|Z_j}(\underline{l}, z_1|1)} \quad (6)$$

$$= l_j + (-1)^{z_1} (l_1 \boxplus l_2 \boxplus \dots \boxplus l_{j-1} \boxplus l_{j+1} \boxplus \dots \boxplus l_d). \quad (7)$$

The outer decoder corrects both the residual bit error of the corrected inner information bits  $z'_1 \neq \hat{z}'_1$  and the bit error of the reliable bit channels  $z_j \neq \hat{z}_j$  for each  $j$ .

Figure 2 shows the decoding performance of 12.9%-OH concatenated (128,120,4)-eBCH-KP4 codes and CP-MLC with (128,113,6)-eBCH and KP4 codes with near MLD, using Chase decoding with the number of test patterns by 1024. The BER of CP-MLC, shown as a solid line, is better than that of concatenated codes because high-OH eBCH codes can be exploited in unreliable bits. On the other hand, an error floor appears in the high SNR region due to the dominant error of bypassed reliable bits in the KP4 BER threshold.

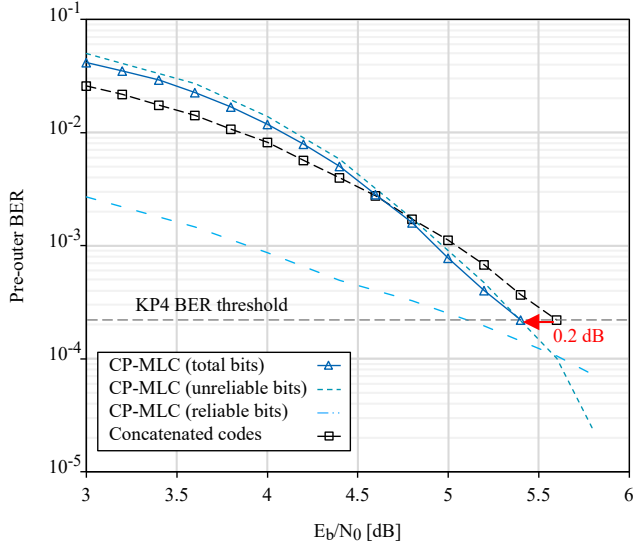


Fig. 2. Pre-outer BER of concatenated codes and CP-MLC [12].

### III. CP-MLC-ID

This section describes the encoder and the iterative decoder for CP-MLC-ID.

#### A. Encoder

We decompose as the information bits as  $z \triangleq (z'_1, z'_2, \dots, z'_{d-1}, z_d)$ . The inner encoder first converts each information bits  $z'_j \in \{0, 1\}^{nR_j/d}$  into  $z_j \in \{0, 1\}^{n/d}$  for each  $1 \leq j \leq d-1$  and  $z_d \in \{0, 1\}^{n/d}$ . Here, the code rate  $R_j$  for each inner code. The bit-interleavers  $S_1, S_2, \dots, S_d$  output the bit-interleaved bits  $\beta_1, \beta_2, \dots, \beta_d \in \{0, 1\}^{n/d}$ , respectively. The CP-MLC-ID codeword is given by

$$\mathbf{b} \triangleq (\beta_1 \oplus \beta_d, \beta_2 \oplus \beta_d, \dots, \beta_{d-1} \oplus \beta_d, \beta_d). \quad (8)$$

#### B. Iterative decoder

CP-MLC-ID uses the iterative decoder to reduce the performance degradation by considering the correlation between unreliable bit channels as similar to bit-interleaved coded modulation with an iterative decoder [18].

On the other side, the iterative decoder with maximum iteration  $I \geq 1$  first calculates the processing loop for  $\forall i \in [1, I]$  and  $j = (i-1 \bmod (d-1)) + 1$ , as follows.

- 1) We calculate the unreliable LLR (uLLR)

$$\lambda_j^{\text{in}} \triangleq l_j \boxplus \tilde{l}_{d,j}, \quad (9)$$

and

$$\tilde{l}_{d,j} \triangleq l_d + \sum_{j'=1:j' \neq j}^{d-1} l_{d,j'}^{\text{ext}}, \quad (10)$$

where  $l_{d,j}^{\text{ext}} = \mathbf{0}$  holds in the first iteration, which is updated in (14).

- 2) The inner decoder  $\mathcal{D}$  calculates a soft-information

$$\lambda_j^{\text{out}} = \mathcal{D}_j(\mathcal{S}_j^{-1}(\lambda_j^{\text{in}})), \quad (11)$$

for each  $1 \leq j \leq d-1$ , and outputs each inner codeword  $\hat{z}_j \triangleq \mathcal{S}^{-1}(\hat{s}_j)$ , where we define  $\hat{s}_j \triangleq 0.5(1 - \text{sign}(\lambda_j^{\text{out}}))$ .

- 3) The extrinsic information  $l_{d,j}^{\text{ext}}$  is updated by

$$l_{d,j}^{\text{ext}} \triangleq l_j \boxplus \lambda_j^{\text{out}} \quad (12)$$

$$\simeq \text{sign}(l_j) \text{sign}(\lambda_j^{\text{out}}) \min(|l_j|, |\lambda_j^{\text{out}}|) \quad (13)$$

$$\simeq \xi[i] l_j (-1)^{\hat{\beta}_j} \quad (14)$$

$$= \underbrace{\xi[i] l_j (-1)^{\hat{\beta}_j}}_{\text{Correctness}} - \underbrace{\xi[i] 2e_j \cdot l_j (-1)^{\hat{\beta}_j}}_{\text{Incorrectness } \Delta_j}, \quad (15)$$

where a bit error is defined by  $e_j = \beta_j \oplus \hat{\beta}_j$  and  $\xi[i]$  is the *damping factor* for each iteration. With the small value of  $\xi[i]$ , the incorrectness  $\Delta_j$  decreases at the cost of fewer correct updates of the LLR  $l_{d,j}^{\text{ext}}$ .

Next, bypassed bits  $\hat{z}_d$  are calculated by

$$\hat{z}_d \triangleq \mathcal{S}_d^{-1}(0.5(1 - \text{sign}(\gamma_d^{\text{in}}))), \quad (16)$$

where rLLR is given by

$$\gamma_d^{\text{in}} \triangleq \sum_{j=1}^{d-1} l_{d,j}^{\text{ext}}. \quad (17)$$

We denote the iterative decoder as shown in Algorithm 1, and give the factor-graph interpretation of the algorithm in subsection III-C.

#### C. Factor graph representation of CP-MLC-ID

We explain the interpretation of the iterative decoder by using the factor graph representation. The factor graph  $\mathcal{G}(\mathcal{V}, \mathcal{C})$  is a bipartite graph with *variable node* (VN)  $\mathcal{V}$  and *check node* (CN)  $\mathcal{C}$  [19]. The two types of messages under  $\mathcal{G}$  are defined by

$$\phi(v, c) \triangleq \sum_{v' \in \mathcal{V}(c) \setminus v} \psi(c, v') \quad (18)$$

and

$$\psi(c, v) \triangleq \boxplus_{c' \in \mathcal{C}(v) \setminus c} \phi(v, c'), \quad (19)$$

where  $\mathcal{C}(v) \subset \mathcal{C}$  and  $\mathcal{V}(c) \subset \mathcal{V}$  are a subset of adjacent nodes for  $v$  and  $c$ , respectively.

We define the VNs of the bit of CP-MLC-ID codewords  $B_j$  and the interleaved bit  $S_j$ . The set of VNs  $\mathcal{V}$  is defined by

$$\mathcal{V} = \{B_1, B_2, \dots, B_d, S_1, S_2, \dots, S_{d-1}\}. \quad (20)$$

---

**Algorithm 1** Calculate iterative decoder  $\hat{z} = \mathcal{D}(l)$

---

**Require:**  $l$

```

1: for  $i = 1, 2 \dots I$  do
2:    $j \leftarrow (i - 1 \bmod (d - 1)) + 1$ 
3:   if  $i = 1$  then
4:      $\tilde{l}_{d,j} \leftarrow l_d$ 
5:   else
6:      $\tilde{l}_{d,j} \leftarrow l_d + \sum_{j'=1:j' \neq j}^{d-1} l_{d,j'}^{\text{ext}}$ 
7:   end if
8:    $\lambda_j^{\text{in}} \leftarrow l_j \boxplus \tilde{l}_j[i]$ 
9:    $\hat{z}_j \leftarrow \mathcal{D}_j(\mathcal{S}_j^{-1}(\lambda_j^{\text{in}}))$ 
10:   $\hat{\beta}_j \leftarrow \mathcal{S}_j(\hat{z}_j)$ 
11:   $l_{d,j}^{\text{ext}} \leftarrow l_j(-1)^{\hat{\beta}_j}$ 
12: end for
13:  $\gamma_d^{\text{in}} \leftarrow \sum_{j=1}^{d-1} l_{d,j}^{\text{ext}}$ 
14:  $\hat{z}_d \leftarrow \mathcal{S}_d^{-1}(0.5(1 - \text{sign}(\gamma_d)))$ 
15:  $\hat{z} \leftarrow (\hat{z}'_1, \hat{z}'_2, \dots, \hat{z}_d)$ 

```

---

We define an indicator function  $\delta(\cdot)$  by

$$\delta(A) \triangleq \begin{cases} 1 & (A \text{ is true}) \\ 0 & (A \text{ is false}) \end{cases}. \quad (21)$$

We define the condition of the parity check matrix for inner codes and XOR in CP-MLC-ID as  $\delta_j \triangleq \delta(\beta_j \oplus \mathbf{b}_j \oplus \mathbf{b}_d = 0)$  and  $\delta_{H_j} \triangleq \delta(H_j z_j = 0)$ , respectively. The CNs of CP-MLC-ID are given by

$$\mathcal{C} = \{\delta_1, \delta_2, \dots, \delta_{d-1}, \delta_{H_1}, \delta_{H_2}, \dots, \delta_{H_{d-1}}\}. \quad (22)$$

We define the message as given by a constant value:

$$\phi(B_j, S_j)[i] = l_j. \quad (23)$$

The CNs of inner codes  $\psi(\delta_{H_j}, S_j)$  are calculated by a SISO decoder. Figure 3 showed the schematic diagram of the factor graph of CP-MLC-ID. The message scheduling of CP-MLC-ID is given by

$$\begin{aligned} &\phi(S_1, \delta_{H_1})[1] \rightarrow \psi(\delta_{H_1}, S_1)[1] \rightarrow \phi(S_1, \delta_1)[1] \rightarrow \psi(\delta_1, B_d)[1] \\ &\rightarrow \phi(B_d, \delta_2)[2] \rightarrow \psi(\delta_2, S_2)[2] \rightarrow \dots \rightarrow \psi(\delta_j, B_d)[I_{\max}], \end{aligned} \quad (24)$$

with  $j = (i - 1 \bmod d - 1) + 1$ . CP-MLC-ID finally calculates the estimated bypass bits  $\hat{z}_d$  from Eq. (16), where  $\gamma_d^{\text{in}} = \sum_{j=1}^{d-1} \psi(\delta_j, B_d)$ . Figure 4 shows the schematic diagram of the decoding procedure with the  $d$  of 3. The decoders of concatenated codes restore the bits from LLRs. On the other hand, CP-MLC-ID updates the  $z_j$  alternately, which corresponds to the message scheduling in Eq. (24), and bypasses one lane.

#### D. Interleaver design

In this subsection, we describe the design of the bit interleaver  $\mathcal{S}_j$ , which mitigates the incorrectness  $\Delta_j$  in the inner codeword  $z_j$ . We first consider the CP-MLC-ID without a bit-interleaver i.e., the interleaver size  $S = 1$ , and using  $d$  of 3,

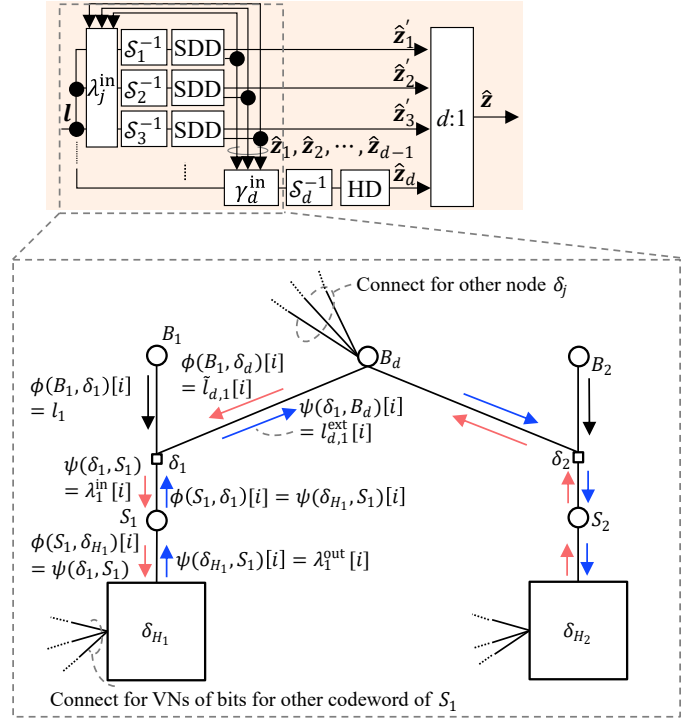


Fig. 3. Schematic diagram for conventional concatenated codes and CP-MLC-ID.

(a) Concatenated codes

(b) CP-MLC-ID

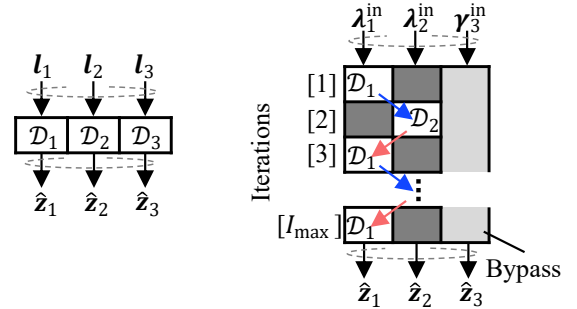


Fig. 4. Schematic flow for (a) concatenated codes and (b) CP-MLC-ID with  $d$  of 3.

as shown in Fig. 5(a). The incorrectness  $\Delta_j$  corresponding to the bit error  $e_j$  propagates to other lanes at the same bit error positions, causing severe performance degradation.

We consider CP-MLC-ID using a simple bit interleaver of size  $S = n$  as shown in Fig. 5(b), where one bit of the codeword with the length of  $n$  is XORed with each bit of  $n$  other codewords. With a simple bit interleaver design, even if the incorrectness  $\Delta_1$  is large, the bit interleaver reduces the effect of error propagation by spreading  $\Delta_2$ .

We also show the CP-MLC-ID using a bit interleaver size of  $S = s$  bits in Fig. 5 (c). The CP-MLC-ID using a bit interleaver with  $S = s$  mitigates the error propagation as a proportion to  $S$ . Figure 6 shows the bit interleaver size dependency for CP-MLC-ID with 3 and 6 iterations using (128, 106, 8)-extended BCH (eBCH) codes and OSD with

832 candidates, where  $(n, k, t)$ -eBCH codes have codeword length  $n$ , information length  $k$ , and minimum distance between codewords  $t$ . Note that the details of the code construction and the selection of candidates for OSD are described in Sec. IV and Appendix A, respectively. CP-MLC-ID with  $S = 1$  using 3 and 6 iterations has an SNR loss of 0.4 and 0.5 dB, respectively, compared to CP-MLC-ID with  $S = 128$ . In contrast, the CP-MLC-ID with  $S = 8$  has an SNR loss of only about 0.1 dB. These findings demonstrate that CP-MLC-ID can improve the decoding performance by using only weak connections between codewords via XOR.

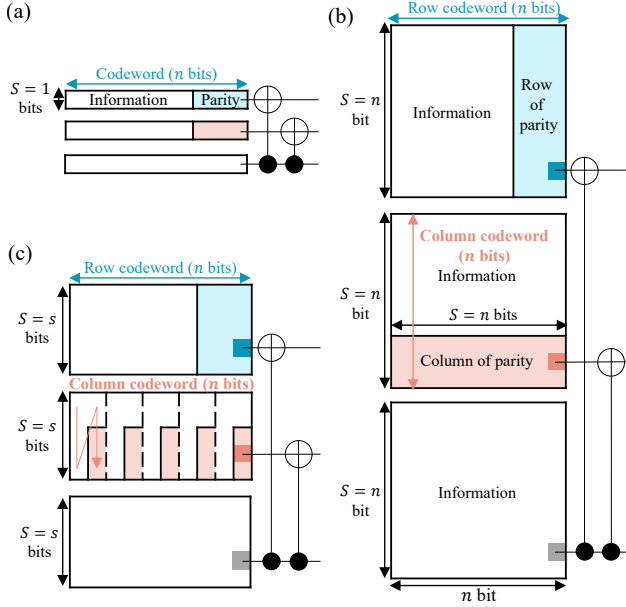


Fig. 5. CP-MLC-ID with  $d = 3$  using bit interleaver size of (a)  $S = 1$  (b)  $S = n$ , and (c)  $S = s$ .

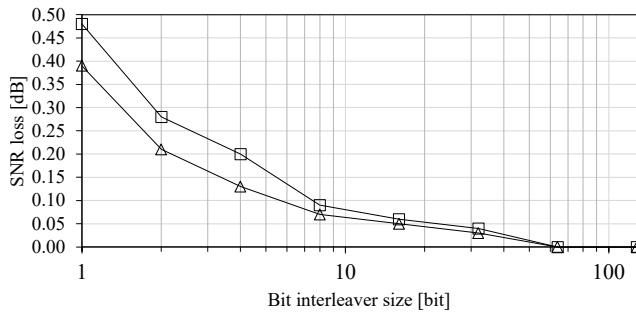


Fig. 6. Decoding performance loss for CP-MLC-ID for each bit interleaver size  $S$ . CP-MLC-ID has 3 and 6 iterations using  $(128, 106, 8)$ -eBCH code and OSD with candidates of  $t = 832$ . We transmit to 300 frames.

#### IV. NUMERICAL SIMULATION

This section describes the numerical simulation we conducted to evaluate the decoding performance.

##### A. Code configuration

We constructed about 19.5% concatenated codes, CP-MLC, and CP-MLC-ID as shown in Table I. The decoding algorithm

of the inner eBCH codes adopts an *ordered statistical decoding* (OSD). The outer code uses 5.56% KP4 codes, which achieves the pre-FEC BER of  $2.2 \times 10^{-4}$  [20].

The concatenated codes, CP-MLC with  $d$  of 2, and CP-MLC-ID with  $d$  of 3 exploit the  $(128, 113, 6)$ -eBCH codes,  $(128, 113, 10)$ -eBCH codes, and  $(128, 113, 8)$ -eBCH codes, respectively. Note that the CP-MLC and CP-MLC-ID can use high-OH eBCH codes by bypassing the half- and one-third bits. CP-MLC-ID has the damping factors  $\xi[i]$  of

$$(\xi[1], \xi[2], \xi[3]) = (0.3, 1.0, 1, 0) \quad (25)$$

and

$$(\xi[1], \xi[2], \xi[3], \xi[4], \xi[5], \xi[6]) = (0.2, 0.3, 0.5, 0.7, 0.9, 1.0), \quad (26)$$

by searching for sub-optimum values in the span of 0.1. Note that the optimization for each  $\xi[i]$  depends on the error probability, the number of candidates of the inner decoder, the target bit error probability, and so on. CP-MLC-ID exploits the bit-interleaver size of  $S = n$  bits.

TABLE I  
CODE CONSTRUCTION WITH OUTER KP4 CODES

Code	Total-OH [%]	Inner codes	OH [%]
Concatenated codes	19.89	$(128, 113, 6)$ -eBCH	13.27
CP-MLC	19.36	$(128, 99, 10)$ -eBCH	29.29
CP-MLC-ID	19.53	$(128, 106, 8)$ -eBCH	20.75

##### B. Numerical simulation results

Figure 7(a) shows that the decoding performance of the concatenated codes, CP-MLC, and CP-MLC-ID, which have  $t = 839$ ,  $t = 825$ , and  $t = 832$  candidates, respectively. CP-MLC-ID has  $I = 3$ , which is equal to the number of SDDs per 3 lanes denoted as  $N_{\text{SDD}}(3) = 3$ . CP-MLC has an error floor caused by the reliable bit channel  $V_j$ , and therefore it cannot exceed the performance of concatenated codes under the KP4-BER threshold. In contrast, CP-MLC-ID outperformed the concatenated codes at the KP4 BER threshold because the inner  $(128, 106, 8)$ -eBCH codes correct a large part of the bit error and keep the error floor low enough by increasing the capacity of reliable bit channel  $U_i$ , compared to the CP-MLC. Note that the error propagation effect of CP-MLC and CP-MLC-ID degrades the BER in high BER regions.

Figure 7(b) show the NCG for concatenated codes, CP-MLC-ID with  $N_{\text{SDD}}(3) = 3$ , and  $N_{\text{SDD}}(3) = 6$ , for each candidate. The NCG of the concatenated codes is saturated as it approaches the MLD performance. The CP-MLC-ID with  $N_{\text{SDD}} = 3$  can improve the decoding performance by 0.25 dB or more compared to the concatenated codes. The CP-MLC-ID with  $N_{\text{SDD}}(3) = 6$  can improve the NCG by 0.4 dB or more by doubling the number of SDDs  $N_{\text{SDD}}(3) = 6$ .

The decoding complexity of CP-MLC-ID consists of the updating  $\lambda_j^n$  (as shown in Eq. (9)), and the bit interleaver, in addition to the SDDs. Equation (9) requires processing in accordance with the times of  $O(n)$  for the boxplus operator. Thus, the updating cannot be ignored in the evaluation of complexity with Eq. (9) when using inner codes with a



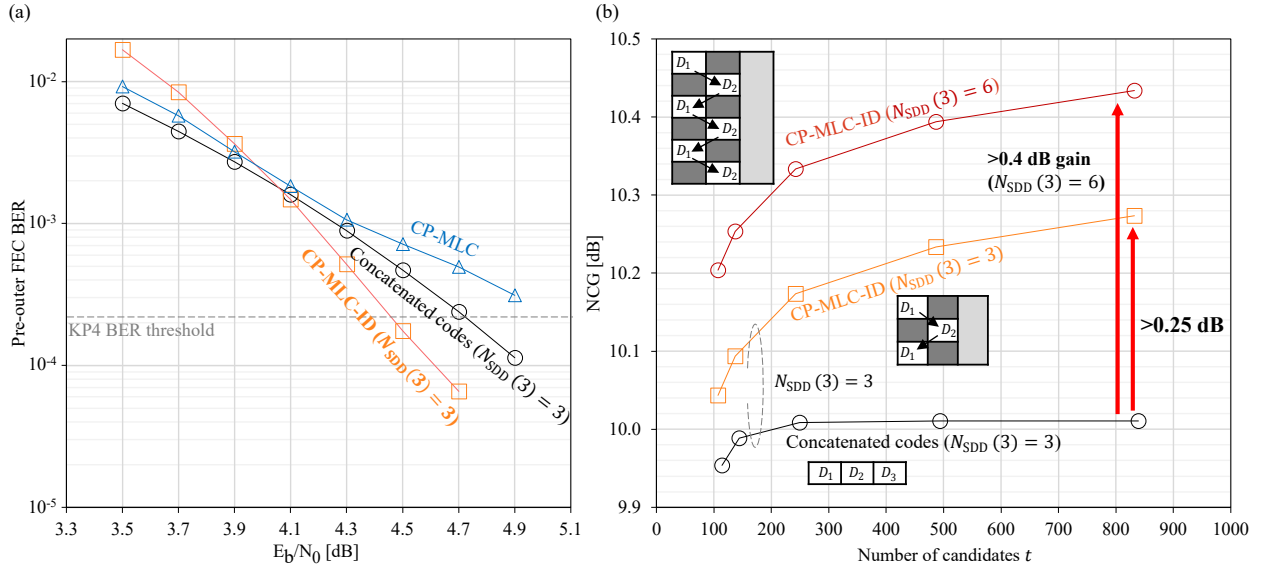


Fig. 7. (a) Decoding performance for concatenated code, CP-MLC, and CP-MLC-ID with number of SDDs  $N_{SDD}(3) = 3$ . (b) NCG versus number of candidates for concatenated codes, CP-MLC-ID with number of SDDs  $N_{SDD}(3) = 3$ , and CP-MLC-ID with number of SDDs  $N_{SDD}(3) = 6$ . Results were first evaluated in [15], [16].

small number of candidates. The bit interleaver also has the potential to become a major contributor to complexity because it requires the shuffling to the LLR, which has 3- to 5-bit quantization. Therefore, the size of the bit interleaver must be carefully designed. Evaluation of complexity and power consumption is difficult without a well-designed and efficient circuit design, which will be the subject of future work.

## V. CONCLUSION

In this paper, we showed that channel-polarized multilevel coding with iterative decoding (CP-MLC-ID) improves the decoding performance under low-complexity SDD. The CP-MLC-ID iteratively corrects the large error by using the high OH inner codes with SDD in the unreliable bit channel, bypassing the SDD in the highly reliable bit channels. CP-MLC-ID outperforms the maximum NCG by up to 0.25 and 0.4 dB for the same number of SDDs and twice the number of SDDs, respectively, compared to concatenated codes, by using only the XOR between the inner codes.

## APPENDIX A

### GENERATION RULE FOR CANDIDATES IN OSD

In this section, we explain how to select codeword candidates for OSD. OSD can order the decoding metric (e.g., LLR  $l$ ) and then convert the code space  $C(G)$  by generating the generator matrix  $G$  into a new code space  $C(G')$  where the parity bit is equal to the position of  $n - k$  linear independent LRBs. The candidate codeword set  $\mathcal{Z}$  is obtained by  $z = (i \oplus t)G'$  for each  $t \in \mathcal{T}$ , which is a *flipping set*. Finally, the OSD outputs the most likely codeword  $\hat{z}$ , which is the minimum Euclidean distance between the decoding metric and  $z \in \mathcal{Z}$ .

The flipping set as *order- $m$*   $\mathcal{T}_m$  consists of flipping  $t$ -bit or less. We define the flipping set as *semi-order- $m$*   $\mathcal{T}_2(m_1, m_2)$ , which selects two bits in the range of

$0, 1, 2, \dots, m_1$  and  $0, 1, 2, \dots, m_2$ , respectively. The number of candidates  $|\mathcal{T}_2(m_1, m_2)|$  is given by

$$|\mathcal{T}_2(m_1, m_2)| = m_1 C_2 - m_2 C_2 \quad (27)$$

In the candidate selection discussed in Sec. IV, we choose the parameters as shown in Tab. II. Note that the parameter is suboptimal, which means that we can improve the performance by optimizing the parameter.

TABLE II  
CANDIDATES FOR OSD

Code	Candidate set $\mathcal{T}$	$ \mathcal{T} $
(128,113,6)-eBCH codes	$\mathcal{T}_0 \cup \mathcal{T}_1$	114
	$\mathcal{T}_0 \cup \mathcal{T}_1 \cup \mathcal{T}_2(10, 4)$	144
	$\mathcal{T}_0 \cup \mathcal{T}_1 \cup \mathcal{T}_2(20, 9)$	249
	$\mathcal{T}_0 \cup \mathcal{T}_1 \cup \mathcal{T}_2(30, 19)$	494
	$\mathcal{T}_0 \cup \mathcal{T}_1 \cup \mathcal{T}_2(40, 29)$	839
(128,106,8)-eBCH codes	$\mathcal{T}_0 \cup \mathcal{T}_1$	107
	$\mathcal{T}_0 \cup \mathcal{T}_1 \cup \mathcal{T}_2(10, 4)$	137
	$\mathcal{T}_0 \cup \mathcal{T}_1 \cup \mathcal{T}_2(20, 9)$	242
	$\mathcal{T}_0 \cup \mathcal{T}_1 \cup \mathcal{T}_2(30, 19)$	487
	$\mathcal{T}_0 \cup \mathcal{T}_1 \cup \mathcal{T}_2(40, 29)$	832
(128,99,10)-eBCH codes	$\mathcal{T}_0 \cup \mathcal{T}_1 \cup \mathcal{T}_2(40, 29)$	825

## REFERENCES

- [1] T. Kupfer, A. Bisplinghof, T. Duthel, C. Fludger, and S. Langenbach, "Optimizing power consumption of a coherent dsp for metro and data center interconnects," in *2017 Optical Fiber Communications Conference and Exhibition (OFC)*, 2017, pp. 1–3.
- [2] *Implementation Agreement for 800LR Coherent Interface*, OIF, 2023.
- [3] "OIF implementation Agreement 400-ZR,OIF-400ZR-01.0," 2020. [Online]. Available: [https://www.oiforum.com/wp-content/uploads/OIF-400ZR-01.0\\_reduced2.pdf](https://www.oiforum.com/wp-content/uploads/OIF-400ZR-01.0_reduced2.pdf)
- [4] H. Sun, T. Veguru, D. Millar, C. Fludger, and R. Maher, "Considerations on FEC Options for 1600ZR & ZR+," 2024, oif2024.231.01. [Online]. Available: <https://www.oiforum.com/bin/c5i?mid=4&rid=7&gid=0&k1=54267&k2=1&k3=11>
- [5] "Power consumption assessment for 1600ZR," 2024. [Online]. Available: <https://www.oiforum.com/bin/c5i?mid=4&rid=7&gid=0&k1=54362>

- [6] “1600ZR link delivered SNR and Modem RSNR,” p. oif2024.389.02, 2024. [Online]. Available: <https://www.oiforum.com/bin/c5i?mid=4&rid=7&gid=0&k1=54439&k2=2&k3=11>
- [7] “Updated link analysis and proposals for 1600ZR,” p. oif2024.448.02, 2024. [Online]. Available: <https://www.oiforum.com/bin/c5i?mid=4&rid=7&gid=0&k1=54498&k2=2&k3=11>
- [8] Y. Polyanskiy, H. V. Poor, and S. Verdú, “Channel coding rate in the finite blocklength regime,” *IEEE Transactions on Information Theory*, vol. 56, no. 5, pp. 2307–2359, 2010.
- [9] D. Chase, “Class of algorithms for decoding block codes with channel measurement information,” *IEEE Transactions on Information Theory*, vol. 18, no. 1, pp. 170–182, 1972.
- [10] M. Fossorier and S. Lin, “Soft-decision decoding of linear block codes based on ordered statistics,” *IEEE Transactions on Information Theory*, vol. 41, no. 5, pp. 1379–1396, 1995.
- [11] K. Tao, Z. Long, W. Qian, Z. Wei, X. Chen, W. Wang, and Y. Xia, “Low-complexity forward error correction for 800g unamplified campus link,” in *2022 20th International Conference on Optical Communications and Networks (ICOON)*, 2022, pp. 1–3.
- [12] T. Kakizaki, M. Nakamura, E. Yamazaki, F. Hamaoka, and Y. Kisaka, “Improved performance-complexity trade-offs for soft-decision decoding by channel-polarized multilevel coding,” in *49th European Conference on Optical Communications (ECOC 2023)*, vol. 2023, 2023, pp. 266–269.
- [13] T. Kakizaki, M. Nakamura, F. Hamaoka, and Y. Kisaka, “Low-complexity channel polarized multilevel coding for modulation-format-independent forward error correction,” in *2021 European Conference on Optical Communication (ECOC)*, 2021, pp. 1–4.
- [14] T. Kakizaki, M. Nakamura, F. hamaoka, and Y. Kisaka, “Channel-Polarized Multilevel Coding for Low-Complexity Forward Error Correction,” *Journal of Lightwave Technology*, pp. 1–9, 2025.
- [15] T. Kakizaki, M. Nakamura, F. Hamaoka, S. Yamamoto, and E. Yamazaki, “Channel-polarized multilevel coding with iterative decoder for net coding gain improvement of short-block-length codes,” in *2024 OptoElectronics and Communications Conference (OECC)*, vol. W4C, 2024.
- [16] T. Kakizaki, E. Nakamura, F. Hamaoka, S. Yamamoto, and E. Yamazaki, “Low-complexity Half-iterative Decoder with Channel-polarized Multilevel Coding for Power Consumption Constrained Data Center Network Application,” in *50th European Conference on Optical Communications (ECOC 2024)*, vol. M2C.1, 2024.
- [17] E. Agrell and M. Secondini, “Information-theoretic tools for optical communications engineers,” in *2018 IEEE Photonics Conference (IPC)*, 2018, pp. 1–5.
- [18] X. Li, A. Chindapol, and J. Ritcey, “Bit-interleaved coded modulation with iterative decoding and 8 psk signaling,” *IEEE Transactions on Communications*, vol. 50, no. 8, pp. 1250–1257, 2002.
- [19] T. Richardson and R. Urbanke, *Modern coding theory*. Cambridge university press, 2008.
- [20] J. Haasz, “IEEE Standard for Ethernet,” *IEEE Std 802.3-2015 (Revision of IEEE Std 802.3-2012)*, pp. 1–4017, 2016.